# Supporting Information

## Chen et al. 10.1073/pnas.1321160111

### SI Text

The following calculation is to exclude the possibility of the presence of interstitial iron or vacant selenium for the extra rows of spot in the [−121] zone-axis pattern (Fig. 2). Assuming the chalcogen height is 1/4 (instead of ∼0.23–0.27) (1–3) of the $c$ lattice parameter, the structure factor of tetragonal $\beta$-$Fe_{1+y}Se_{1-x}$ could be expressed as

$$\begin{aligned}
F(\theta) &= \sum_i^{\infty} f_{Se} e^{2\pi i(hx_i+ky_i+lz_i)} + \sum_i^{\infty} f_{Fe} e^{2\pi i(hx_i+ky_i+lz_i)} \\
&= x\left(f_{Se} e^{2\pi i\left(0h+\frac{1}{2}k+\frac{1}{4}l\right)} + f_{Se} e^{2\pi i\left(\frac{1}{2}h+0k+\frac{3}{4}l\right)}\right) \\
&\quad + f_{Fe} e^{2\pi i(0h+0k+0l)} + f_{Fe} e^{2\pi i\left(\frac{1}{2}h+\frac{1}{2}k+0l\right)} \\
&\quad + y\left(f_{Fe} e^{2\pi i\left(\frac{1}{2}h+0k+\frac{1}{4}l\right)} + f_{Fe} e^{2\pi i\left(0h+\frac{1}{2}k+\frac{3}{4}l\right)}\right) \\
&= \left\{x \cdot f_{Se}\left(e^{\pi i\left(k+\frac{1}{2}l\right)} + e^{\pi i\left(h+\frac{3}{2}l\right)}\right) + f_{Fe}\left(1+e^{\pi i(h+k)}\right)\right\} \\
&\quad + y \cdot f_{Fe}\left(e^{\pi i\left(h+\frac{1}{2}l\right)} + e^{\pi i\left(k+\frac{3}{2}l\right)}\right),
\end{aligned}$$

where $x$ and $y$ are concentrations of Se vacancy and Fe interstitial atom, respectively. If hkl = 111, then

$$\begin{aligned}
F(\theta) &= \left\{x \cdot f_{Se}\left(e^{\pi i\left(1+\frac{1}{2}\right)} + e^{\pi i\left(1+\frac{3}{2}\right)}\right) + f_{Fe}\left(1+e^{\pi i(1+1)}\right)\right\} \\
&\quad + y \cdot f_{Fe}\left(e^{\pi i\left(1+\frac{1}{2}\right)} + e^{\pi i\left(1+\frac{3}{2}\right)}\right) \\
&= x \cdot f_{Se}(-i+i) + f_{Fe}(1+1) + y \cdot f_{Fe}(-i+i) = 2f_{Fe},
\end{aligned}$$

which means that the {111} reflections are independent of both Se vacancy and the Fe interstitial atom. Thus, the spots between 000 and 111 shown by the white arrows in Fig. 2*B* must result from other modulations. The previously reported ordering of Fe vacancies in $A_{1-x}Fe_{2-y}Se_2$ with the forms of $\sqrt{5} \times \sqrt{5} \times 1$ (4), $\sqrt{2} \times \sqrt{2} \times 1$ (5), $\sqrt{2} \times 2\sqrt{2} \times 1$ (6), and $\sqrt{8} \times \sqrt{10} \times 1$ (7) could be excluded because these systematic rows of spots implied a structural modulation every doubled interplanar spacing along [111] direction.

The $\beta$-$Fe_3Se_4$ particle analyzed in this study was very close to the [−131] zone axis when we found it. Five selected area electron diffraction (SAED) patterns were taken. When the particle was tilted back to the initial [−131] zone axis (tilting process 2 in Fig. S2*A*), the readings of the X- and Y-tilt of the double-tilting specimen holder were deviated from the initial values when the [−131] zone-axis pattern was taken by about 1.2°. This inconsistency may result from the instability between the particle and the supporting thin carbon film. Inhomogeneous local heating from the electron beam illumination may cause the particle to rotate with respect to the specimen holder. The instability is also confirmed by tracing the rotation of (101) spots between all of the zone-axis patterns (Table S3). This phenomenon may be one of the reasons that some of the angles between zone-axis patterns in Table S2 show considerable deviations from the tetragonal $\beta$-FeSe.


1. McQueen TM, et al. (2009) Extreme sensitivity of superconductivity to stoichiometry in Fe1+delta Se. *Phys Rev B* 79(1):014522.
2. Pomjakushina E, Conder K, Pomjakushin V, Bendele M, Khasanov R (2009) Synthesis, crystal structure, and chemical stability of the superconductor FeSe1-x. *Phys Rev B* 80(2):024517.
3. Joseph B, et al. (2010) Evidence of local structural inhomogeneity in FeSe1-xTex from extended x-ray absorption fine structure. *Phys Rev B* 82(2):020502.
4. Zavalij P, et al. (2011) Structure of vacancy-ordered single-crystalline superconducting potassium iron selenide. *Phys Rev B* 83(13):132509.
5. Wang Z, et al. (2011) Microstructure and ordering of iron vacancies in the superconductor system K_{y}Fe_{x}Se_{2} as seen via transmission electron microscopy. *Phys Rev B* 83(14):140505.
6. Yan YJ, et al. (2012) Electronic and magnetic phase diagram in K(x)Fe(2-y)Se(2) superconductors. *Sci Rep* 2:212.
7. Ding X, et al. (2013) Influence of microstructure on superconductivity in $KxFe_{2-y}Se_2$ and evidence for a new parent phase $K_2Fe_7Se_8$. *Nat Commun* 4:1897.

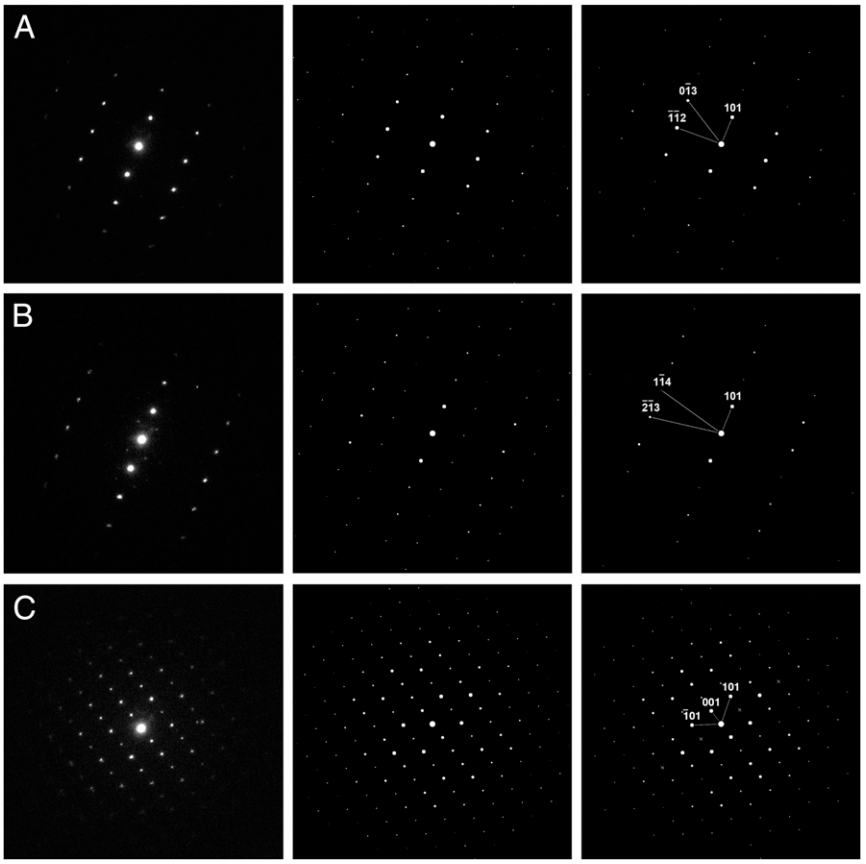


**Fig. S1.** From *Left* to *Right*: experimental SAED and simulated kinematical electron diffraction (KED) patterns of $\beta$-$Fe_3Se_4$ and $\beta$-FeSe in the zone axes of (*A*) [−131], (*B*) [−151], and (*C*) [010].

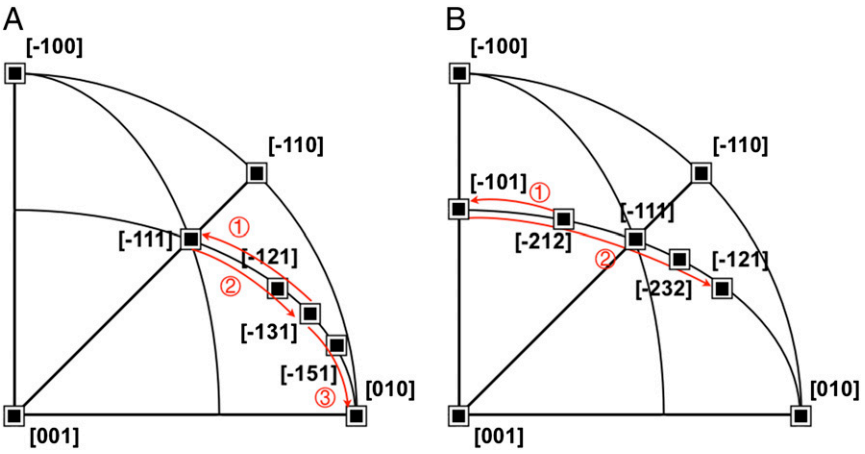


**Fig. S2.** Stereographic projections of the plane normals (circles) and zone axes (squares) of $\beta$-FeSe (solid symbol, hkl) showing the specimen tilting progress based on the combined SAED patterns in (*A*) Fig. 3. and (*B*) Fig. 4.

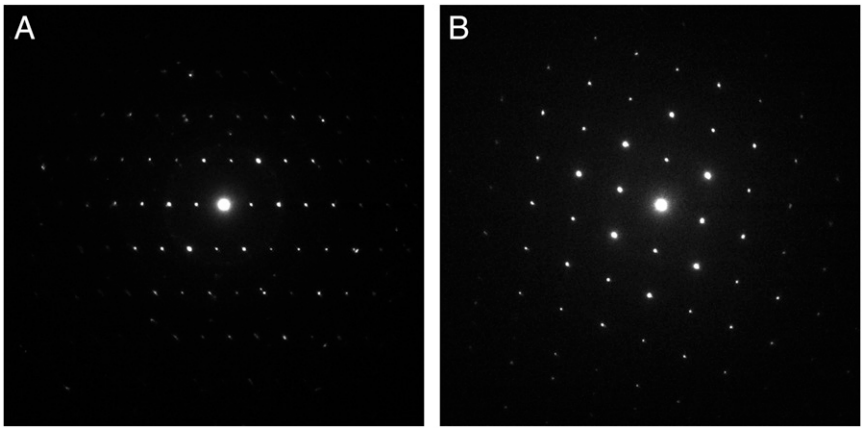


**Fig. S3.** Experimental SAED patterns of $\beta$-$Fe_3Se_4$ prepared by an aqueous chemical route in the zone axes of (*A*) [−121] and (*B*) [−111]. The lattice parameters are $a = 3.98(7)$ Å and $c = 5.18(14)$ Å, about 5% elongation along the *a* and *b* axes, and 6% shrinkage along the *c* axis compared with the tetragonal $\beta$-FeSe. The deformation is much different from the $\beta$-$Fe_3Se_4$ prepared by a high-pressure route (Fig. 3).

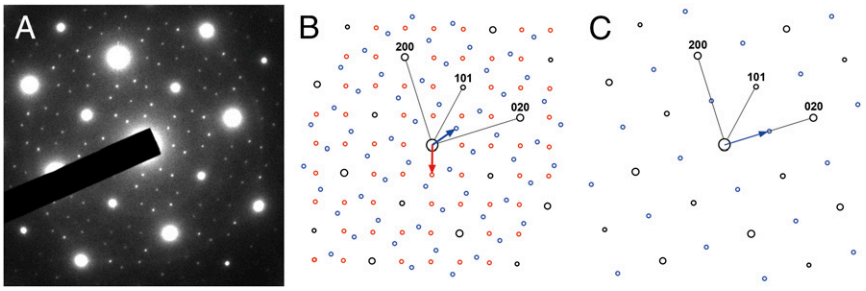


**Fig. S4.** (*A*) Experimental SAED and simulated KED patterns of (*B*) twinned $\beta$-$Fe_4Se_5$ and (*C*) $\beta$-$Fe_3Se_4$ in the zone axis of [001].

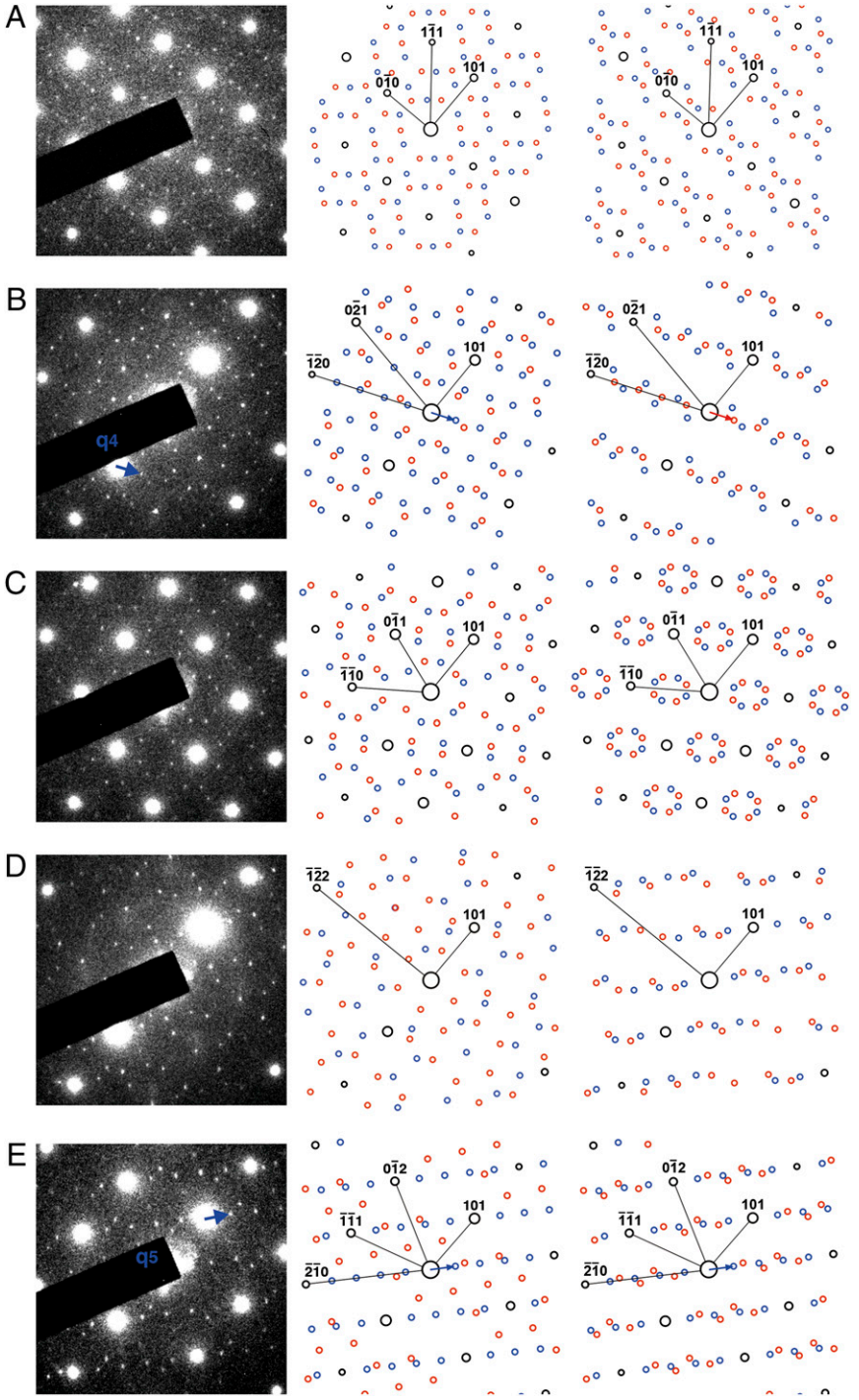


**Fig. S5.** From *Left* to *Right*: experimental SAED and simulated KED patterns of twinned $\beta$-$Fe_9Se_{10}$ with and without $1/2d_{310}$ shift every other (001) plane in the zone axes of (*A*) [−101], (*B*) [−212], (*C*) [−111], (*D*) [−232], and (*E*) [−121]. Superstructure wave vectors $\mathbf{q}_4 = (1/5, 2/5, 0)$ and $\mathbf{q}_5 = (2/5, 1/5, 0)$ are indicated by blue arrows.

**Table S1. Observed and calculated d-spacings for $\beta$-$Fe_3Se_4$**

| | d-spacings (Å) | | |
|---|---|---|---|
| hkl | Observed | Calculated | Refined |
| 001 | 5.71 | 5.53 | 5.70 |
| 100 | 3.65 | 3.78 | 3.67 |
| 101 | 3.08 | 3.12 | 3.09 |
| 110 | 2.60 | 2.67 | 2.60 |
| 102 | 2.25 | 2.23 | 2.25 |
| 112 | 1.93 | 1.92 | 1.92 |
| 201 | 1.74 | 1.79 | 1.75 |
| 103 | 1.69 | 1.66 | 1.69 |
| 211 | 1.56 | 1.61 | 1.58 |
| 213 | 1.24 | 1.24 | 1.24 |
| 114 | 1.25 | 1.23 | 1.25 |
| 310 | 1.17 | 1.19 | 1.16 |

The observed d-spacings were obtained from the SAED patterns in Fig. 3. The calculated d-spacings were based on the lattice parameters ($a$ = 3.765 Å and $c$ = 5.518 Å) of synthetic bulk $\beta$-FeSe at room temperature (1). The refined d-spacings for the present $\beta$-$Fe_3Se_4$ [for $a$ = 3.67(1) Å and $c$ = 5.70 (1) Å] are also given.

1. Okamoto H (1991) The Fe-Se (iron-selenium) system. *J Phase Equilibria* 12(3):383–389.

**Table S2. Observed and calculated interzone-axis angles for $\beta$-$Fe_3Se_4$ and bulk $\beta$-FeSe (1)**

| | Angles (°) | | |
|---|---|---|---|
| Interzone axes | Observed ($\beta$-$Fe_3Se_4$)* | Calculated ($\beta$-$Fe_3Se_4$)† | Calculated ($\beta$-FeSe) |
| [131]Λ[121] | 11.23 | 9.11 | 9.21 |
| [121]Λ[111] | 19.45 | 19.20 | 19.26 |
| [131]Λ[151] | 10.03 | 8.25 | 8.37 |
| [151]Λ[010] | 19.85 | 13.38 | 13.61 |

*Tilting angles between zone-axis patterns are calculated from the X- and Y-tilt of the double tilt analytical electron microscopy (AEM) specimen holder.
†Calculated from refined $\beta$-$Fe_3Se_4$ lattice in Table S1.

1. Okamoto H (1991) The Fe-Se (iron-selenium) system. *J Phase Equilibria* 12(3):383–389.

**Table S3. Angles for all (101) diffraction spots deviated (rotated) from those in the [−131] zone-axis pattern**

| Zone axis | Angles (°) |
|---|---|
| [−131] | — |
| [−121] | 0.24 |
| [−111] | 3.67 |
| [−151] | 0.70 |
| [010] | 3.03 |

Positive values represent rotations toward counterclockwise direction.

**Table S4. Crystal structure parameters of $\beta$-$Fe_3Se_4$, $\beta$-$Fe_4Se_5$, and $\beta$-$Fe_9Se_{10}$ used for generating kinematical electron diffraction patterns**

| Atom | $x$ | $y$ | $z$ |
|---|---|---|---|
| $\beta$-$Fe_3Se_4$ | Space group no. 121: $I\bar{4}2m$ | | |
| | $a$ = 5.19 Å | $c$ = 11.40 Å | |
| Fe(1) | 0.5 | 0 | 0 |
| Fe(1) | 0.5 | 0.5 | 0 |
| Fe(2) | 0 | 0 | 0 |
| Se | 0.25 | 0.25 | 0.13 |
| $\beta$-$Fe_4Se_5$ | Space group no. 75: P4 | | |
| | $a$ = 8.41 Å | $c$ = 5.47 Å | |
| Fe(1) | 0.2 | 0.1 | 0 |
| Fe(1) | 0.3 | 0.4 | 0 |
| Fe(2) | 0.5 | 0 | 0 |
| Se | 0 | 0 | 0.26 |
| Se | 0.2 | 0.6 | 0.26 |
| Se | 0.1 | 0.3 | 0.74 |
| Se | 0.5 | 0.5 | 0.74 |
| $\beta$-$Fe_9Se_{10}$ | Space group no. 86: $P4_2/n$ | | |
| | $a$ = 8.41 Å | $c$ = 10.94 Å | |
| Fe(1) | 0.3 | 0.1 | 0 |
| Fe(1) | 0.5 | 0.5 | 0 |
| Fe(1) | 0.2 | 0.4 | 0 |
| Fe(2) | 0 | 0 | 0 |
| Se | 0.5 | 0 | 0.13 |
| Se | 0.1 | 0.2 | 0.13 |
| Se | 0.4 | 0.3 | 0.87 |

No refinement to the experimental electron diffraction patterns was performed. Fe(2) represents iron vacancies.